Journal of Control, Automation and Electrical Systems (2020) 31:1063–1073
https://doi.org/10.1007/s40313-020-00592-x

Closed-Form Approximation for Horizontal Grounding Electrodes Transient Analysis

Rodolfo A. R. Moura[1] · Marco Aurélio O. Schroeder[1] · Antonio C. S. Lima[2] · Pedro H. N. Vieira[1]

Received: 19 April 2019 / Revised: 1 December 2019 / Accepted: 31 March 2020 / Published online: 22 April 2020
© Brazilian Society for Automatics–SBA 2020

Abstract
The method of moments (MoM) is widely used in several areas of knowledge to solve integral equations. In the specific case of solving electrical grounding transient behavior problems, the computational time is usually high. This paper presents new alternative solutions for solving the double integrals in the well-known hybrid electromagnetic model (HEM) applied to horizontal grounding electrodes. These new alternative solutions correspond to using an approximation to the exponential term appearing in the finite integral needed to obtain the parameters. Two approaches are considered either using Maclaurin series or Padé approximation. The corresponding results are compared with those obtained by using HEM with MoM. It is shown that the proposed solutions allow reducing the computational time, without jeopardizing accuracy.

Keywords Method of moments · Numerical methods · Grounding · Transient analysis

1 Introduction

The low-frequency response of electrical grounding systems is relatively well characterized in the literature (IEEE Std. 80-2000 2000). However, when requested by impulsive currents, grounding systems may present a very complex transient response. A physically consistent modeling requires that the electromagnetic field for the specific grounding system geometry is correctly evaluated and that the soil behavior is correctly accounted for. This behavior includes the frequency dependence of the soil electrical parameters, conductivity and permittivity and soil ionization, for high amplitude currents (Smith-Rose 1933; Scott 1966; Scott et al. 1967; Longmire and Smith 1975; Portela 1999; Alipio and Visacro 2013, 2014b; Liew and Darveniza 1974; Ala et al. 2008; Otani et al. 2014; He and Zhang 2015; Liu et al. 2017; Mokhtari and Gharehpetian 2018; Kherif et al. 2018; Chen and Du 2019; Sekioka 2019). Several methodologies are presented in literature allowing to deal with these matters (Dawalibi 1986a, b; Grcev and Dawalibi 1990; Grcev 2009; Dawalibi and Selby 1993; Visacro and Soares 2005; Karami et al. 2017; Ding et al. 2017; Tanaka et al. 2018; Clavel et al. 2018; Karami and Sheshyekani 2018; Lima et al. 2018; Razi-Kazemi and Hajian 2018; Sunjerga et al. 2019; Grcev et al. 2018; Rizk et al. 2019; Kherif et al. 2019; Gholinezhad and Shariatinasab 2019; Grcev et al. 2019; Lima et al. 2019; Ramamoorty et al. 1989; Otero et al. 1999; Verma and Mukhedkar 1980; Mazzetti and Veca 1983; Velzaquez and Mukhedkar 1984; Tanabe 2001; Tsumura et al. 2006; Alipio et al. 2011, 2012a; Magalhães et al. 2015).

Concerning the electromagnetic field evaluation, the published methodologies can be grouped in three major groups: (i) circuit theory approach (Kherif et al. 2018; Sekioka 2019; Ramamoorty et al. 1989; Otero et al. 1999), (ii) transmission line theory (Chen and Du 2019; Ding et al. 2017; Grcev et al. 2018, 2019; Verma and Mukhedkar 1980; Mazzetti and Veca 1983; Velzaquez and Mukhedkar 1984) and (iii) full-wave theory either in the frequency domain or time domain (Portela 1999; Dawalibi 1986a, b; Grcev and Dawalibi 1990; Grcev 2009; Dawalibi and Selby 1993; Visacro and Soares 2005; Karami et al. 2017; Tanaka et al. 2018; Clavel et al. 2018; Karami and Sheshyekani 2018; Lima et al. 2018; Razi-Kazemi and Hajian 2018; Sunjerga et al. 2019; Grcev et al. 2018; Rizk et al. 2019; Gholinezhad and Shariatinasab 2019;

✉ Antonio C. S. Lima
acsl@dee.ufrj.br

Rodolfo A. R. Moura
moura@ufsj.edu.br

[1] Electrical Engineering Department, Federal University of São João del-Rei, Pça. Frei Orlando, 170 - Centro, São João del-Rei, MG 36307-352, Brazil

[2] Department of Electrical Engineering, Federal University of Rio de Janeiro, Rio de Janeiro, Brazil

Grcev et al. 2019; Lima et al. 2019; Tanabe 2001; Tsumura et al. 2006). Each methodology presents advantages and disadvantages (Alipio et al. 2011, 2012a) that are basically reflected on accuracy and computational time. For example, the circuit theory approach normally requires low computational effort, but cannot model properly fast transients, such as lightning. Models based on line theory assume that the propagation of the electromagnetic field, guided by the grounding electrode, is dictated by the transverse electromagnetic propagation mode (TEM). Methods based on full-wave theory are the most physically consistent, being able to model phenomena within the frequency spectrum range from 100 Hz up to 1–4 MHz (Magalhães et al. 2015). However, they are the most difficult to implement and consume the largest computational time.

The well-known hybrid electromagnetic model (HEM) (Visacro and Soares 2005; Visacro and Portela 1992; Visacro et al. 2002) is highlighted due to: (i) its relatively easy implementation, (ii) its validation by comparison with experimental results (Visacro et al. 2011; Visacro and Alipio 2012; Alipio and Visacro 2014a; Visacro et al. 2014) and (iii) its wide application for transient studies in transmission line systems, including grounding (Visacro and Silveira 2015, 2016; Silveira and Visacro 2014). The numerical solution of HEM involves computing double integrals. This solution is often obtained by using the method of moments (MoM). However, the computational time is high. The main reasons for the very long processing time of the HEM consist of the necessity of: (i) getting solutions for a very large number of frequencies and (ii) subdividing the grounding into a relatively large number of segments. This requires running the computational mode repeatedly. The aim of this paper is to present new alternative solutions to overcome the need to solve a complex double integral on evaluating the HEM solution for horizontal grounding electrodes. This is achieved by applying a Maclaurin series or a Padé approximation to the term $\exp(-\gamma r)$, thus leading to an analytical solution of the double integrals. These new alternative solutions allow a substantial reduction of the computational time without jeopardizing accuracy.

2 Horizontal Grounding Electrode Modeling

2.1 Hybrid Electromagnetic Model (HEM)

The so-called HEM (Visacro and Soares 2005; Visacro and Portela 1992; Visacro et al. 2002) consists of: (i) discretizing the grounding electrode into cylindrical segments (thin wire approximation); (ii) obtaining, for each segment, an average potential (V) as function of the transversal current (I_{T}) and a voltage drop (ΔV) as function of the longitudinal current (I_{L}), given the grounding system geometry and soil electromagnetic parameters; (iii) applying electrical circuit theory to determine the node (segments intersection) voltages. Computation is carried out in frequency domain. The node voltages allow determining all the quantities of interest, such as transverse and longitudinal currents, potential and voltage drop and harmonic impedance. (Visacro and Soares 2005; Visacro and Portela 1992; Visacro et al. 2002). The time domain quantities are determined via the inverse Fourier transform. More details on HEM, as well as its validation by comparison with experimental results, can be found, for example, in Visacro and Soares (2005); Visacro and Silveira (2004).

Circuit theory application in HEM is based on considering each segment as a source and evaluating its self and mutual effects. The average potential V_{RS} in the receptor segment associated with the transversal current I_{TS} in the source segment S and the voltage drop ΔV_{RS} along R associated with the longitudinal current I_{LS} in S are given by:

$$V_{\mathrm{RS}} = \frac{1}{4\pi[\sigma(\omega) + j\omega\varepsilon(\omega)]\ell_{\mathrm{S}}\,\ell_{\mathrm{R}}} \int_{\ell_{\mathrm{S}}} \int_{\ell_{\mathrm{R}}} I_{\mathrm{TS}} \frac{e^{-\gamma r}}{r} \mathrm{d}l_{\mathrm{R}}\,\mathrm{d}l_{\mathrm{S}} \tag{1}$$

$$\Delta V_{\mathrm{RS}} = -\frac{j\omega\mu}{4\pi} \int_{\ell_{\mathrm{S}}} \int_{\ell_{\mathrm{R}}} I_{\mathrm{LS}} \frac{e^{-\gamma r}}{r} \overrightarrow{\mathrm{d}l_{\mathrm{R}}} \bullet \overrightarrow{\mathrm{d}l_{\mathrm{S}}} \tag{2}$$

where ℓ_{S} and ℓ_{R} are the segment lengths; r is the distance between the infinitesimal segments $\mathrm{d}l_{\mathrm{S}}$ and $\mathrm{d}l_{\mathrm{R}}$; $\sigma(\omega)$, $\epsilon(\omega)$ and μ are the conductivity, permittivity and permeability of the soil, respectively; $\omega = 2\pi f$ is the angular frequency; $\gamma = \sqrt{j\omega\mu[\sigma(\omega) + j\omega\epsilon(\omega)]}$ is the propagation constant. Note that the possibility of considering the frequency dependence of the soil electrical conductivity and permittivity is considered. For most soils, the magnetic permeability is quite close to that of the vacuum ($\mu = \mu_0$) (Portela 1999).

As the grounding electrodes are found close to a boundary of two half-spaces (earth and air), to implement the influence of this interface the method of images is used (Arnautovski-Toseva and Grcev 2016; Grcev and Grceva 2009).

To avoid dealing with an integral equation, the MoM is usually used leading to an algebraic problem (Alipio et al. 2011, 2012a, b; Schroeder et al. 2017). The solution is based on the well-known Gauss–Legendre integration that presents a good accuracy for just a low quadrature order. The authors implemented this numerical technique for solving HEM equations to compare results with those obtained using the proposed new alternative solutions. Results shown in this paper were obtained using order 4 (resulting into 16 points) as the solution of the double integral that must be computed.

2.2 Transversal and Longitudinal Impedance Evaluation

The transversal and longitudinal currents I_{TS} and I_{LS} vary from segment to segment. However, within each segment these currents are considered uniform and used to define the elements of transversal and longitudinal impedance matrices, Z_{TRS} and Z_{LRS}:

$$V_{RS} = Z_{TRS} I_{TS} \tag{3}$$

$$\Delta V_{RS} = Z_{LRS} I_{LS} \tag{4}$$

Taking into consideration the interface between air and soil, another segment source is placed parallel to the first one (Arnautovski-Toseva and Grcev 2016; Grcev and Grceva 2009). Therefore, it is possible to obtain matrices of total transversal and longitudinal impedances (including the contributions of the sources and their respective images):

$$Z_{Ttotal} = Z_{TRS} + Z_{TRS-IMAGE} \tag{5}$$

$$Z_{Ltotal} = Z_{LRS} + Z_{LRS-IMAGE} \tag{6}$$

The following new alternative solutions are derived for horizontal electrodes of radius a and length ℓ and buried in the soil at a depth d. The xx axis is considered along the electrode, with origin at the current injection point.

2.3 New Alternative Solution Using Maclaurin Series

The Maclaurin expansion of the $\exp(-\gamma r)$ term is considered:

$$e^{-\gamma r} = \sum_{n=0}^{\infty} \frac{(-\gamma r)^n}{n!} \tag{7}$$

Replacing (7) in (1) and (2), the following analytical solutions are obtained for the mutual elements of Z_T and Z_L (Sect. 6.1):

$$Z_{TRS} = \frac{1}{4\pi[\sigma(\omega) + j\omega\varepsilon(\omega)]\ell_S\ell_R}(m_A + m_B) \tag{8}$$

$$Z_{LRS} = -\frac{j\omega\mu_0}{4\pi}(m_A + m_B) \tag{9}$$

with m_A and m_B given by:

$$m_A = \left\{ \begin{array}{l} x_{RO} \ln\left(\left|\frac{x_{RO}-x_{SI}}{x_{RO}-x_{SO}}\right|\right) + x_{RI} \ln\left(\left|\frac{x_{RI}-x_{SO}}{x_{RI}-x_{SI}}\right|\right) \\ x_{SO} \ln\left(\left|\frac{x_{RO}-x_{SO}}{x_{RI}-x_{SO}}\right|\right) + x_{SI} \ln\left(\left|\frac{x_{RI}-x_{SI}}{x_{RO}-x_{SI}}\right|\right) \end{array} \right\} \tag{10}$$

$$m_B = \sum_{n=1}^{\infty} \frac{(-\gamma)^n}{n(n+1)n!} \left\{ \begin{array}{r} |x_{RI}-x_{SO}|^{n+1} \\ -|x_{RI}-x_{SI}|^{n+1} \\ -|x_{RO}-x_{SO}|^{n+1} \\ +|x_{RO}-x_{SI}|^{n+1} \end{array} \right\} \tag{11}$$

where x_{SO} and x_{SI} are, respectively, the positions at the beginning and ending of the source segment S; x_{RO} and x_{RI} are similar, but for the receptor segment R.

For the self-elements ($S \equiv R$), the approximation $\exp(-\gamma r) \approx 1$ is generally accepted, as the effect of propagation can be disregarded (Salari and Portela 2007). Equations (8) and (9) can be used with $(m_A + m_B) \approx \ell_R m_p$:

$$m_P = 2\left[\ln\left(\frac{\sqrt{1+\left(\frac{a}{\ell_S}\right)^2}+1}{\frac{a}{\ell_S}}\right) - \sqrt{1+\left(\frac{a}{\ell_S}\right)^2} + \frac{a}{\ell_S}\right] \tag{12}$$

For $Z_{TRS-IMAGE}$ and $Z_{LRS-IMAGE}$, equations similar to Eqs. (8) to (12) can be derived. The distances between the source and receptor segments become: $r_{RO_{IMAGE}}$ (instead of x_{RO}) and $r_{RI_{IMAGE}}$ (instead of x_{RI}), and the following approximations are considered:

$$r_{RO\,IMAGE} \approx x_{RO} + 2d \tag{13}$$

$$r_{RI\,IMAGE} \approx x_{RI} + 2d \tag{14}$$

The loss of accuracy associated with these approximations varies from segments to segments, and it will depend on the electrode length ℓ and on the depth d.

As regards the number of terms n to be used in the Maclaurin series, two alternatives are considered: (a) using a convergence test of the series, with 1% criteria, and (b) using just the first term, that is, $n = 1$, thus resulting $\exp(-\gamma r) = 1 - \gamma r$. Results obtained with the alternatives (a) and (b) are identified by the labels PS and $PS_{n=1}$, respectively.

2.4 New Alternative Solution Using Padé Approximation

Another alternative solution is obtained by using the Padé approximation:

$$e^{-\gamma r} = \left(1 - \frac{\gamma r}{2}\right) \Big/ \left(1 + \frac{\gamma r}{2}\right) \tag{15}$$

Replacing (15) in (1) and (2), the following analytical solutions are obtained (Sect. 6.2):

$$Z_{TRS} = \frac{1}{4\pi[\sigma(\omega) + j\omega\varepsilon(\omega)]\ell_S\ell_R}(m_C + m_D) \tag{16}$$

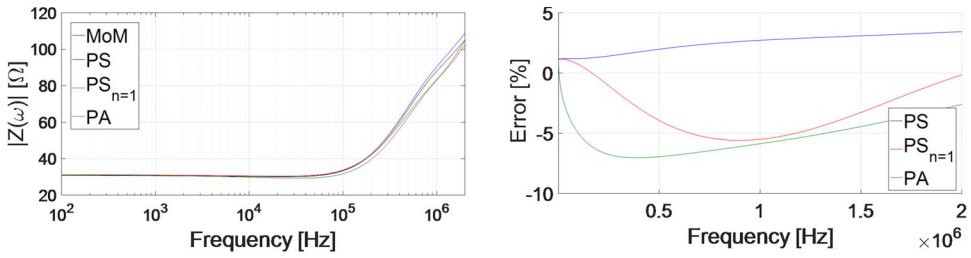

(a) $d = 0.5\,m$; $\ell = 35\,m$; $\rho = 600\,\Omega\,m$ and $\varepsilon_r = 15$

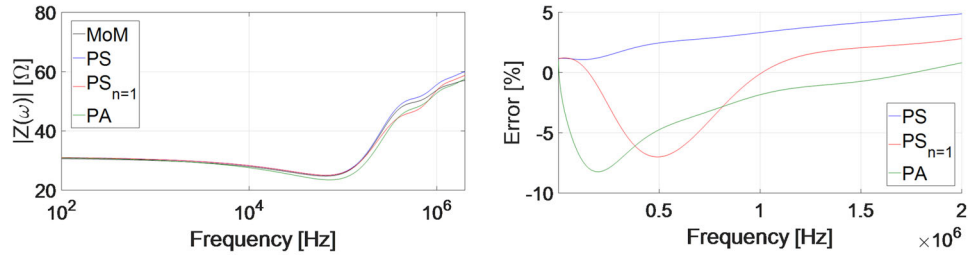

(b) $d = 0.5\,m$; $\ell = 35\,m$; $\rho(\omega)$ and $\varepsilon_r(\omega)$

Fig. 1 $|Z(\omega)|$ and associated errors as compared to MoM results. Base case parameters

$$Z_{\mathrm{LRS}} = -\frac{j\,\omega\,\mu_0}{4\,\pi}\,(m_{\mathrm{C}} + m_{\mathrm{D}}) \tag{17}$$

where m_{C} and m_{D} can be given by:

$$m_C = \left\{\begin{array}{r} -x_{\mathrm{RI}}.\ln\left(|x_{\mathrm{SO}} - x_{\mathrm{RI}}|\right) \\ +x_{\mathrm{RI}}.\ln\left(|x_{\mathrm{SI}} - x_{\mathrm{RI}}|\right) \\ +x_{\mathrm{SO}}.\ln\left(|x_{\mathrm{RI}} - x_{\mathrm{SO}}|\right) \\ -x_{\mathrm{SI}}.\ln\left(|x_{\mathrm{RI}} - x_{\mathrm{SI}}|\right) \end{array}\right\} + \left\{\begin{array}{r} -2x_{\mathrm{SO}}.\ln\left(|2+\gamma(x_{\mathrm{SO}} - x_{\mathrm{RI}})|\right) \\ +\dfrac{2(\gamma x_{\mathrm{RI}} - 2).\ln\left(|2+\gamma(x_{\mathrm{SO}} - x_{\mathrm{RI}})|\right)}{\gamma} \\ \dfrac{-2(\gamma x_{\mathrm{RI}} - 2).\ln\left(|2+\gamma(x_{\mathrm{SI}} - x_{\mathrm{RI}})|\right)}{\gamma} \\ +2x_{\mathrm{SI}}.\ln\left(|2+\gamma(x_{\mathrm{SI}} - x_{\mathrm{RI}})|\right) \end{array}\right\} \tag{18}$$

$$m_{\mathrm{D}} = -\left\{\begin{array}{r} -x_{\mathrm{RO}}.\ln\left(|x_{\mathrm{SO}} - x_{\mathrm{RO}}|\right) \\ +x_{\mathrm{RO}}.\ln\left(|x_{\mathrm{SI}} - x_{\mathrm{RO}}|\right) \\ +x_{\mathrm{SO}}.\ln\left(|x_{\mathrm{RO}} - x_{\mathrm{SO}}|\right) \\ -x_{\mathrm{SI}}.\ln\left(|x_{\mathrm{RO}} - x_{\mathrm{SI}}|\right) \end{array}\right\} - \left\{\begin{array}{r} -2x_{\mathrm{SO}}.\ln\left(|2+\gamma(x_{\mathrm{SO}} - x_{\mathrm{RO}})|\right) \\ +\dfrac{2(\gamma x_{\mathrm{RO}} - 2).\ln\left(|2+\gamma(x_{\mathrm{SO}} - x_{\mathrm{RO}})|\right)}{\gamma} \\ \dfrac{-2(\gamma x_{\mathrm{RO}} - 2).\ln\left(|2+\gamma(x_{\mathrm{SI}} - x_{\mathrm{RO}})|\right)}{\gamma} \\ +2x_{\mathrm{SI}}.\ln\left(|2+\gamma(x_{\mathrm{SI}} - x_{\mathrm{RO}})|\right) \end{array}\right\} \tag{19}$$

Concerning the self-elements ($S \equiv R$), Eq. (12) is also obtained for m_{P}. Moreover, the same procedure as in Sect. 2.3 is used for obtaining $Z_{\mathrm{TRS-IMAGE}}$ and $Z_{\mathrm{LRS-IMAGE}}$. Results obtained with this alternative are identified by the label PA.

3 Accuracy and Computation Time Tests

3.1 Case Studies

The base case study corresponds to a horizontal electrode, with radius $a = 1$ cm and buried at depth $d = 0.5$ m, in a soil with $\rho_0 = 600\ \Omega$ m (low-frequency resistivity). The electrode length ℓ is considered equal to the effective length ($\ell_{\mathrm{ef}} = 35$ m). Other values of the depth (0.02 and 2 m), electrode length (10, 20, 50 and 60 m) and low-frequency soil resistivity (100 and 1000 Ω m) are also considered. The electrode lengths 20 and 50 m are near to the effective length corresponding to 100 and 1000 Ω m soil resistivity values, respectively.

In all cases, two soil models are considered: (i) frequency-independent soil parameters, ρ_0 and $\varepsilon_r = 15$ (relative permittivity), and (ii) frequency-dependent soil parameters, according to Alipio–Visacro model (Alipio and Visacro 2014a) (Sect. 6.3). Also, soil ionization is disregarded. To ensure comparability, all routines were written by the same programmer and the final algorithms compared. Besides, the same system was simulated 100 times to guarantee a convergence on the average values of computational time. It was used a computer with I7-3770 (3.4 GHz) processor and 12-GB RAM. All simulations took place on Windows 8.1 PRO operating systems.

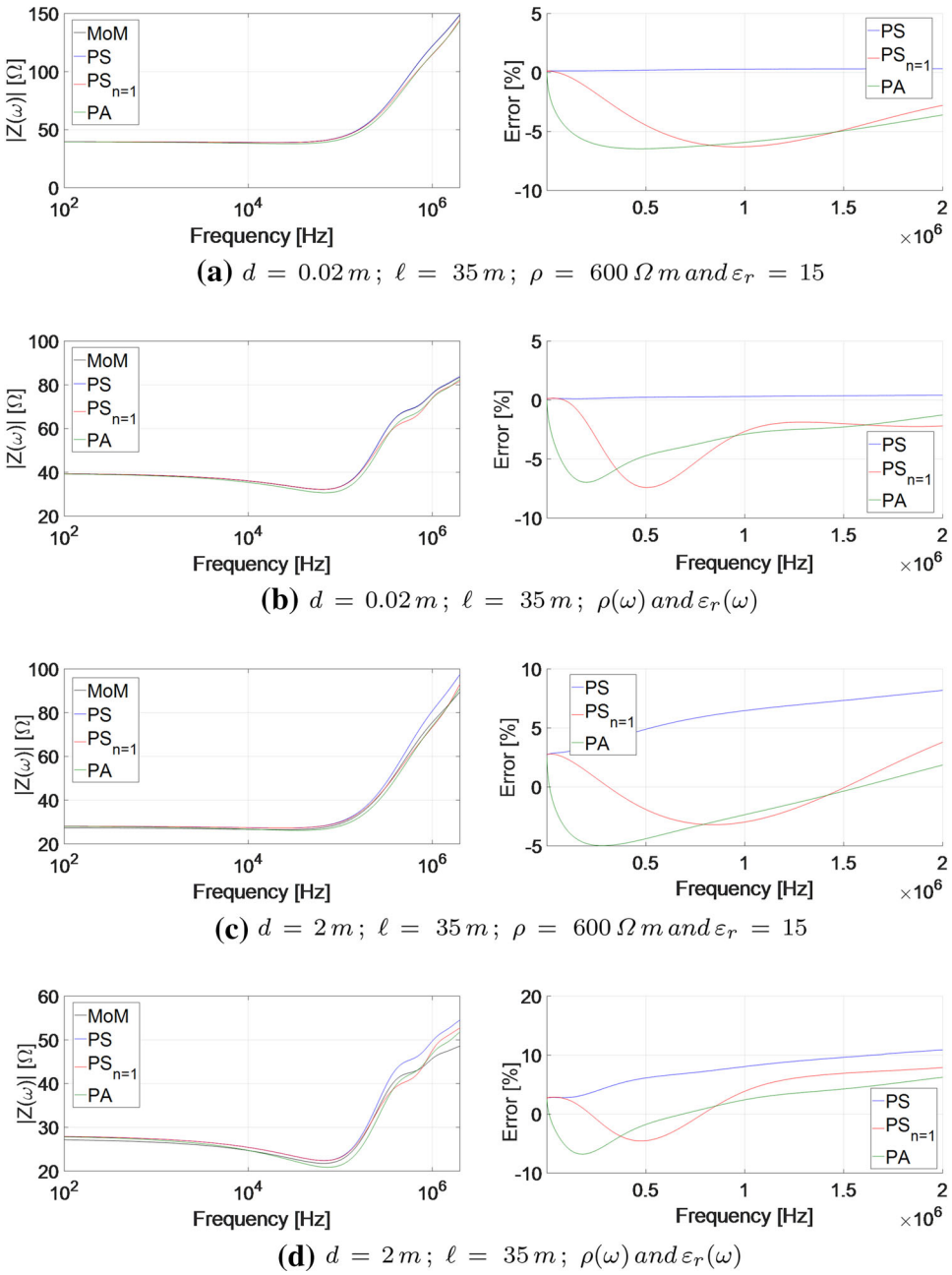

Fig. 2 $|Z(\omega)|$ and associated errors as compared to MoM results. Different depth cases

(a) $d = 0.02\,m$; $\ell = 35\,m$; $\rho = 600\,\Omega\,m$ *and* $\varepsilon_r = 15$

(b) $d = 0.02\,m$; $\ell = 35\,m$; $\rho(\omega)$ *and* $\varepsilon_r(\omega)$

(c) $d = 2\,m$; $\ell = 35\,m$; $\rho = 600\,\Omega\,m$ *and* $\varepsilon_r = 15$

(d) $d = 2\,m$; $\ell = 35\,m$; $\rho(\omega)$ *and* $\varepsilon_r(\omega)$

3.2 Accuracy Tests

The harmonic impedance is used to evaluate the accuracy of the new alternative solutions, when compared to results obtained using MoM. Overall, the computed results show that the proposed solutions generate physically consistent results for the modulus and argument of the harmonic impedance. Results for $|Z(\omega)|$ are presented here.

In Figs. 1, 2, 3 and 4, results obtained using MoM, PS, PS$_{n=1}$ and PA are compared, for the base case (Fig. 1), and depict the influence of parameters d (Fig. 2), ℓ (Fig. 3) and ρ_0 (Fig. 4). The extreme parameter values mentioned in Sect. 3.1 were considered, so to better evaluate their influence. Results in Fig. 5 correspond to practical cases where the effective electrode length is considered for the different soil resistivity values: $\rho_0 = 600\,\Omega\,\text{m} \Rightarrow \ell_{\text{ef}} = 35$ m (Fig. 5a, b), $\rho_0 = 100\,\Omega\,\text{m} \Rightarrow \ell_{\text{ef}} = 20$ m (Fig. 5c, d) and $\rho_0 = 1000\,\Omega\,\text{m} \Rightarrow \ell_{\text{ef}} = 50$ m (Fig. 5e, f). The relative errors associated with using the new alternative solutions are also shown. Figures on the left correspond to considering frequency-independent soil parameters, and the ones on the right correspond to considering frequency-dependent soil parameters.

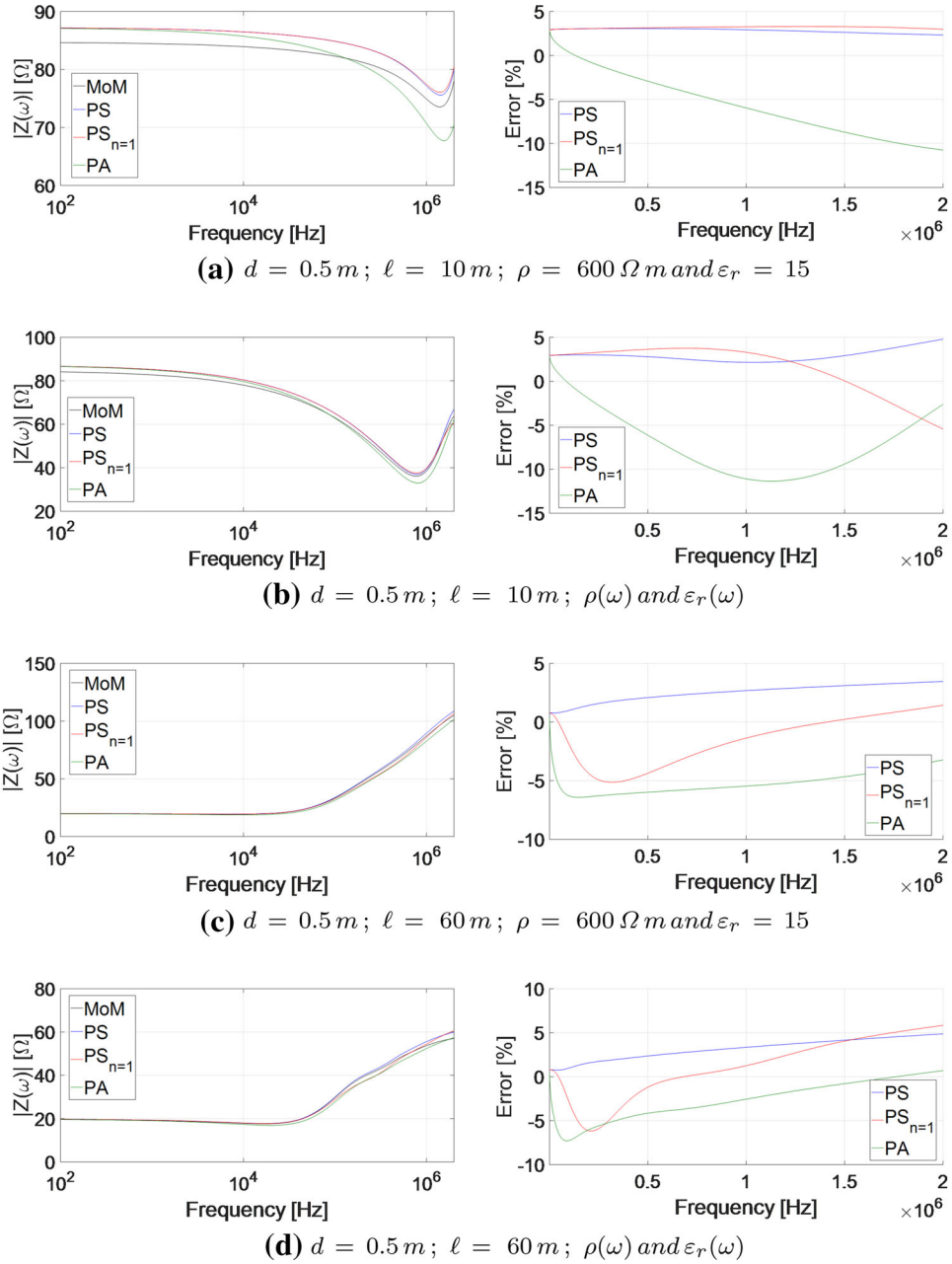

Fig. 3 $|Z(\omega)|$ and associated errors as compared to MoM results. Different length cases

The harmonic impedance was used to compute the grounding potential rise (GPR):

$$\text{GPR} = F^{-1}\{Z(\omega)\, F[i(t)]\} \tag{20}$$

where $i(t)$ is the current that requests the electrode; F and $F^{-}1$ correspond, respectively, to the direct and inverse Fourier transform. Considering a lightning current characteristic of a first stroke, it was found that, although the maximum harmonic impedance error is about 10%, the maximum GPR error is around 5%. Equal or lower errors will be obtained for other quantities that characterize the transient behavior of grounding electrodes, such as the transient impedance, impulse impedance, effective length and impulse coefficient.

3.3 Computation Time

To evaluate the computational efficiency of the new alternative solutions, their computation time is compared to the one corresponding to MoM. Results for all cases represented in Figs. 1 and 2 are presented in Table 1. The positive values of the computational efficiency illustrate the gain obtained by using the new alternative solutions. In general, the lowest computational gain is obtained with PS (the most accurate alternative solution) and the highest gain is obtained with

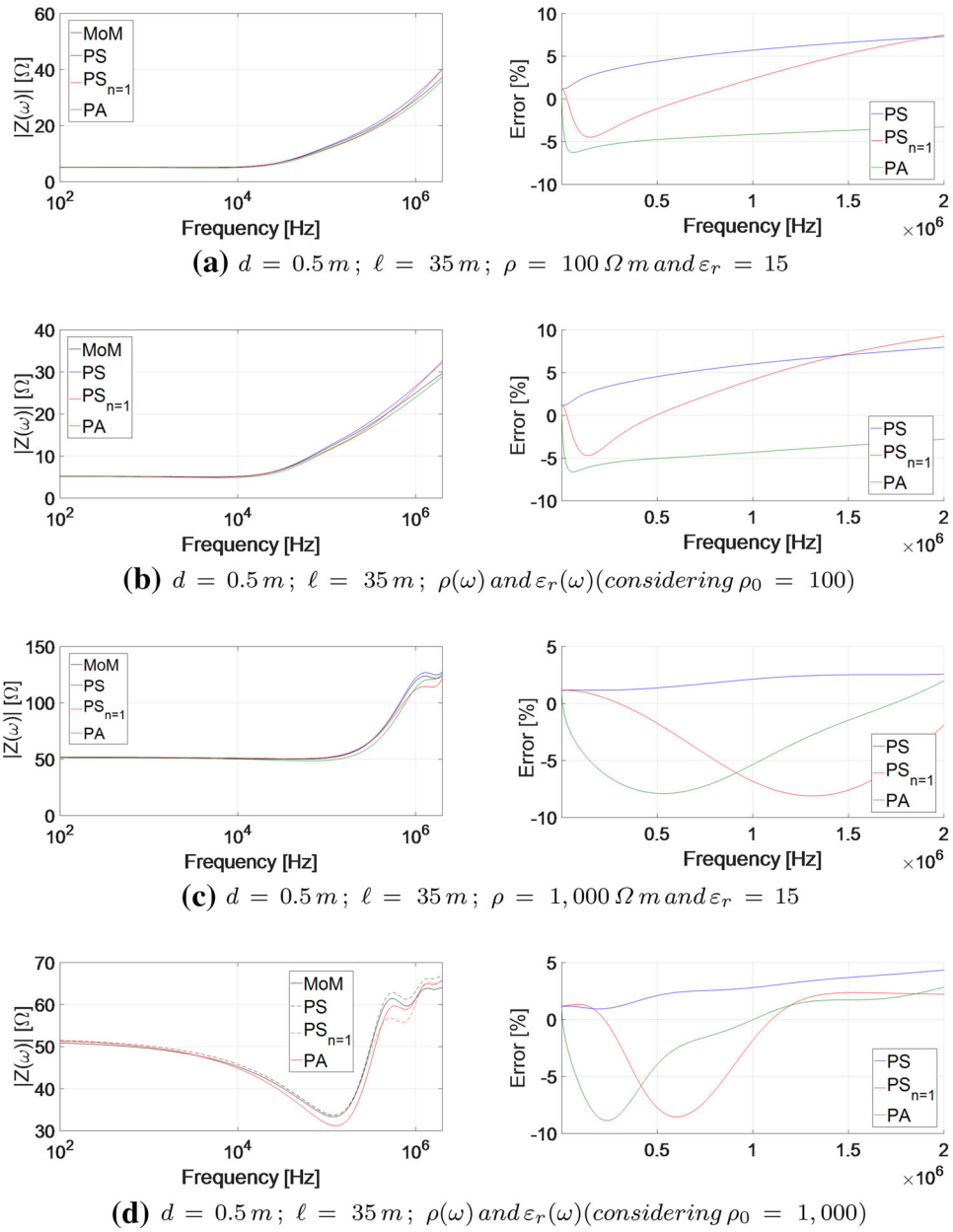

(a) $d = 0.5\,m$; $\ell = 35\,m$; $\rho = 100\,\Omega\,m$ and $\varepsilon_r = 15$

(b) $d = 0.5\,m$; $\ell = 35\,m$; $\rho(\omega)$ and $\varepsilon_r(\omega)$ (considering $\rho_0 = 100$)

(c) $d = 0.5\,m$; $\ell = 35\,m$; $\rho = 1,000\,\Omega\,m$ and $\varepsilon_r = 15$

(d) $d = 0.5\,m$; $\ell = 35\,m$; $\rho(\omega)$ and $\varepsilon_r(\omega)$ (considering $\rho_0 = 1,000$)

Fig. 4 $|Z(\omega)|$ and associated errors as compared to MoM results. Different soil resistivities cases

$PS_{n=1}$, as expected, given that only one term of the Maclaurin series is considered.

For instance, for the base case, the gain obtained by algorithms PS, $PS_{n=1}$ and PA is, respectively, 31%, 119% and 52% faster than the traditional MoM.

Additionally, results in Table 1 of the PS solution show that as the number of terms to meet the convergence criterion increases with the electrode length and the decrease with the soil resistivity value, the computational efficiency of this solution follows the same pattern.

The computational efficiency of PS is very sensitive to the soil model, being higher for frequency-independent soil parameters since the frequency dependence decreases the resistivity values.

In very special cases, the PS solution requires more computation time than the MoM (negative values of the computational efficiency). This occurs for cases that are not realistic from a practical point of view (electrodes much longer than the effective length).

4 Discussion

The results presented here indicate that:

– In all cases, from an engineering perspective, errors using any of the new alternative solutions are acceptable, the maximum error being around 10%.

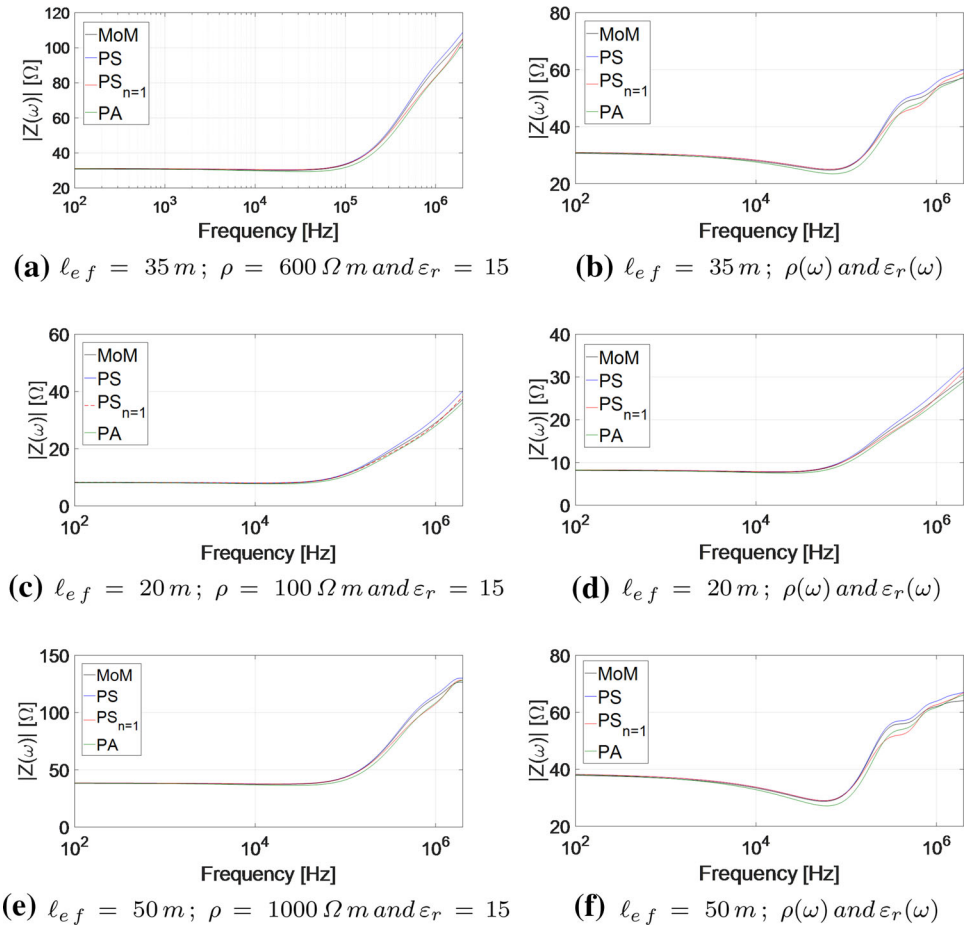

Fig. 5 $|Z(\omega)|$ and associated errors as compared to MoM results, considering the electrode effective length for different soil resistivity values: Curves on the left correspond to frequency-independent soil parameters and on the right to frequency-dependent soil parameters. **a**, **b**—base case parameters; **c**, d—low-resistivity soil; **e**, **f** high resistivity soil. All cases buried at 0.5 m above the ground

– When comparing results obtained with frequency-independent and frequency-dependent soil models, it is clear that the new alternative solutions can reproduce: (i) the decrease in $|Z(\omega)|$ when frequency-dependent parameters are considered; (ii) the increase in the capacitive effect, which can be observed by the decrease in $|Z(\omega)|$ in an intermediate frequency range. These effects of considering the frequency dependence of soil parameters are more accentuated for higher resistivity soils and are more evident in cases (a) (a′), (b) (b′), (c) (c′), (g) (g′) and (i) (i′).
– In general, the PS solution is more accurate, followed by PS$_{n=1}$ and finally by PA. For practical cases, ℓ being close to the effective length (Fig. 2), the maximum error is about 7.5% using PA.
– The largest errors of the PS solution occur at very high frequencies (above 1 MHz), while those corresponding to PS$_{n=1}$ and PA vary over the analyzed frequency band.
– The errors are sensitive to the depth d, being smaller for smaller values of d. This is explained by the approximations (13) and (14), which are more accurate for lower values of d. For $d = 0.5$ m (widely used in practice), the maximum errors are around 7.5% for PS$_{n=1}$ and PA, while for PS, it is reduced to about 3.5%.
– Errors are sensitive to the electrode length ℓ, increasing as ℓ decreases. This is also explained by the approximations (13) and (14), which are more accurate for higher values of ℓ, tending to stabilize for very high frequencies.
– Errors are sensitive to the soil resistivity ρ_0, especially for the solutions PS$_{n=1}$ and PA. In these cases, errors increase with increasing ρ_0. This is due to the fact that, having a lower conductivity soil, the propagation is relevant until a longer distance, along the electrode, and solutions PS$_{n=1}$ and PA reproduce wave propagation less accurately.

5 Conclusions

In field theory-based methods for determining the transient behavior of grounding electrodes, the MoM is commonly used leading to a double integral involving the term $\exp(-\gamma r)$ which can cause a poor convergence and be a numerically demanding task. Aiming at a computational improvement, new alternative solutions for horizontal electrodes are presented in this paper: using Maclaurin series with a convergence criterion (PS) or just the first term (PS$_{n=1}$) and the Padé approximation (PA).

Table 1 Computational efficiency of the new alternative solutions, considering frequency-independent/frequency-dependent soil parameters

Computational efficiency (%) New alternative solution				
Case		Maclaurin (PS)	Maclaurin ($PS_{n=1}$)	Padé (PA)
Fig. 1	(a)	+31	+119	+52
	(b)	+15	+113	+52
Fig. 2	(a)	+33	+116	+53
	(b)	+14	+115	+49
	(c)	+21	+116	+49
	(d)	+6	+113	+47
Fig. 3	(a)	+49	+103	+18
	(b)	+42	+105	+16
	(c)	+4	+55	+30
	(d)	−9	+52	+25
Fig. 4	(a)	−13	+117	+44
	(b)	−13	+120	+54
	(c)	+41	+118	+54
	(d)	+25	+114	+56
Fig. 5	(c)	+14	+138	+48
	(d)	+6	+139	+42
	(e)	+21	+74	+43
	(f)	+2	+75	+36

The results obtained are promising as the harmonic impedance $Z(\omega)$, computed up to 2 MHz, via any of the new alternative solutions, when compared to the results obtained using MoM, presented a maximum difference about 10%, even if considering extreme values of the electrode length and depth, for different soil resistivity values. The computational gain by using PA or $PS_{n=1}$, instead of MoM, is significant, reaching on average, about 40% and 125%, respectively. For practical cases, where the electrode length is related to the soil resistivity value, the efficiency gain is in the order of 70% to 140%. When using PS, the computational gain depends on the electrode depth and length and on the soil resistivity value. It also depends on the used soil model.

Acknowledgements This study was financed in part by the Coordenação de Aperfeiçoamento de Pessoal de Nível Superior—Brasil (CAPES), Finance Code 001. It was also partially supported by Instituto Nacional de Energia Elétrica (INERGE); Fundação de Amparo à Pesquisa do Estado do Rio de Janeiro (FAPERJ) and Conselho Nacional de Pesquisa e Desenvolvimento (CNPq).

6 Appendix

6.1 Maclaurin Series

Replacing (7) in (1) and (2), and given that the electrode is along the xx axis ($\mathrm{d}l_S = \mathrm{d}x_S$, $\mathrm{d}l_R = \mathrm{d}x_R$ and $r = |x_R - x_S|$), the following analytical solutions are obtained for the mutual elements Z_{TRS}:

$$Z_{TRS} = K(\omega) \int_{x_{S0}}^{x_{SI}} \int_{x_{R0}}^{x_{RI}} \frac{1}{|x_R - x_S|} \{1 - \gamma(|x_R - x_S|) + \frac{[\gamma(|x_R - x_S|)]^2}{2!} - \ldots\} \mathrm{d}x_R \mathrm{d}x_S \quad (21)$$

where $K(\omega) = \frac{1}{4\pi[\sigma(\omega) + j\,\omega\,\varepsilon(\omega)]\,\ell_S\,\ell_R}$.

Note that in Eq. (21):

i The first term of the integrand has an analytic solution of the logarithm type, thus resulting in (10) for m_A;
ii The other terms have a polynomial-type solution, leading to (11) for m_B.

To obtain $Z_{TRS-IMAGE}$, the procedure is similar, with $r = \sqrt{(|x_R - x_S|)^2 + (2d)^2}$. Then,

$$Z_{TRS-IMAGE} = K(\omega) \int_{x_{S0}}^{x_{SI}} \int_{x_{R0}}^{x_{RI}} \frac{1}{\sqrt{(|x_R - x_S|)^2 + (2d)^2}} \{1 - \gamma\left(\sqrt{(|x_R - x_S|)^2 + (2d)^2}\right) + \frac{[\gamma\left(\sqrt{(|x_R - x_S|)^2 + (2d)^2}\right)]^2}{2!} - \ldots\} \mathrm{d}x_R \mathrm{d}x_S \quad (22)$$

An analytical solution to (22) is possible if it is assumed that $r = \sqrt{(|x_R - x_S|)^2 + (2d)^2} \approx |x_R - x_S| + 2d$; then, (22) becomes similar to (8).

The same procedure can be used for Z_{LRS} and $Z_{LRS-IMAGE}$ since $\mathrm{d}\vec{l}_S = \mathrm{d}x_S\hat{a}_x$ and $\mathrm{d}\vec{l}_R = \mathrm{d}x_R\hat{a}_x$, see (1) and (2).

6.2 Padé Approximation

Replacing (15) in (1) and (2), the following analytical solutions are obtained:

$$Z_{TRS} = K(\omega) \int_{x_{S0}}^{x_{SI}} \int_{x_{R0}}^{x_{RI}} \frac{1}{|x_R - x_S|} \left[\frac{1 - \frac{\gamma(|x_R - x_S|)}{2}}{1 - \frac{\gamma(|x_R - x_S|)}{2}}\right] \mathrm{d}x_R \mathrm{d}x_S \quad (23)$$

The integral of (23) has analytical solution, as expressed by (16), (19) and (19).

In a similar way, it is possible to obtain $Z_{TRS-IMAGE}$ considering the same approximation used in Sect. 6.1 ($r \approx |x_R - x_S| + 2d$).

For the self-elements, it is possible to approximate $\exp(-\gamma r) \approx 1$ and (12) is obtained according to Salari and

Portela (2007), both for the Maclaurin series and for the Padé approximation.

6.3 Frequency-Dependent Soil Parameters

The frequency-dependent soil parameter model presented in Alipio and Visacro (2014a) is considered:

$$\sigma(\omega) = \sigma_0 + \sigma_0 h(\sigma_0) \left(\frac{f}{10^6}\right)^{\alpha} \tag{24}$$

$$\varepsilon_r(\omega) = \frac{\varepsilon_\infty}{\varepsilon_0} + \frac{\tan(0.5\,\pi\,\alpha) \times 10^{-3}}{2\pi\varepsilon_0 \left(10^6\right)^{\alpha}} \sigma_0 h(\sigma_0) f^{\alpha-1} \tag{25}$$

where $\sigma(\omega)$ is the soil conductivity (in mS/m); $\sigma_0 = 1/\rho_0$ is the low-frequency ground conductivity (in mS/m) measured at 100 Hz; $\varepsilon_r(\omega)$ is the relative soil permittivity. Considering the statistical dispersion of the frequency dependence of soil parameters, the following mean values are adopted: $\alpha = 0.54$, $h(\sigma_0) = 1.26\sigma_0^{-0.73}$ and $\varepsilon_\infty/\varepsilon_0 = 12$ (relative permittivity at higher frequencies).

References

Ala, G., Buccheri, P., Romano, P., & Viola, F. (2008). Finite difference time domain simulation of earth electrodes soil ionisation under lightning surge condition. *IET Science Measurement Technology*, *2*(3), 134–145.

Alipio, R. S., Afonso, M. M., Oliveira, T. A. S., & Schroeder, M. A. O. (2011). Modeling of electrical grounding for high-frequency phenomena and comparison with experimental results. *Revista Controle & Automação*, *22*(1), 89–102. (in Portuguese).

Alipio, R. S., Afonso, M. M., Oliveira, T. A. S., & Schroeder, M. A. O. (2012a). Impulse response of ground electrodes. *Revista Controle & Automação*, *23*(4), 476–488. (in Portuguese).

Alipio, R. S., Schroeder, M. A. O., Afonso, M. M., Oliveira, T. A. S., & Assis, S. C. (2012b). Electric fields of grounding electrodes with frequency dependent soil parameters. *Electric Power Systems Research*, *83*, 220–226.

Alipio, R. S., & Visacro, S. (2013). Frequency depedence of soil parameters: Effect on the lightning response of grounding electrodes. *IEEE Transactions on Power Delivery*, *55*(1), 132–139.

Alipio, R. S., & Visacro, S. (2014a). Modeling the frequency dependence of electrical parameters of soil. *IEEE Transactions on Electromagnetic Compatibility*, *27*(2), 927–935.

Alipio, R., & Visacro, S. (2014b). Impulse efficiency of grounding electrodes: Effect of frequency dependent soil parameters. *IEEE Transactions on Power Delivery*, *29*(2), 716–723.

Arnautovski-Toseva, V., & Grcev, L. (2016). On the image model of a buried horizontal wire. *IEEE Transactions on Electromagnetic Compatibility*, *58*(1), 278–286.

Chen, H., & Du, Y. (2019). Lightning grounding grid model considering both the frequency-dependent behavior and ionization phenomenon. *IEEE Transactions on Electromagnetic Compatibility*, *61*(1), 157–165.

Clavel, E., Roudet, J., Guichon, J.-M., Gouichiche, Z., Joyeux, P., & Derbey, A. (2018). A nonmeshing approach for modeling grounding. *IEEE Transactions on Electromagnetic Compatibility*, *60*(3), 795–802.

Dawalibi, F. (1986a). Electromagnetic fields generated by overhead and buried short conductors, part I-Single conductor. *IEEE Transactions on Power Delivery*, *1*(4), 105–111.

Dawalibi, F. (1986b). Electromagnetic fields generated by overhead and buried short conductors, part II–Ground networks. *IEEE Transactions on Power Delivery*, *1*(4), 112–119.

Dawalibi, F., & Selby, A. (1993). Electromagnetic fields of energized condutors. *IEEE Transactions on Power Delivery*, *8*(3), 1275–1284.

Ding, W.-Y., Wei, X.-C., Yi, D., & Shu, Y.-F. (2017). A closed-form solution for the impedance calculation of grid power distribution network. *IEEE Transactions on Electromagnetic Compatibility*, *59*(5), 1449–1456.

Gholinezhad, J., & Shariatinasab, R. (2019). Time-domain modeling of tower-footing grounding systems based on impedance matrix. *IEEE Transactions on Power Delivery*, *34*(3), 910–918.

Grcev, L. (2009). Impulse efficiency of ground electrodes. *IEEE Transactions on Power Delivery*, *24*(1), 441–451.

Grcev, L., & Dawalibi, F. (1990). An electromagnetic model for transients in grounding systems. *IEEE Transactions on Power Delivery*, *5*(4), 1773–1781.

Grcev, L., & Grceva, S. (2009). On HF circuit models of horizontal grounding electrodes. *IEEE Transactions on Electromagnetic Compatibility*, *51*(3), 873–875.

Grcev, L., Kuhar, A., Markovski, B., & Arnautovski-Toseva, V. (2019). Generalized network model for energization of grounding electrodes. *IEEE Transactions on Electromagnetic Compatibility*, *61*(4), 1082–1090.

Grcev, L. D., Kuhar, A., Arnautovski-Toseva, V., & Markovski, B. (2018). Evaluation of high-frequency circuit models for horizontal and vertical grounding electrodes. *IEEE Transactions on Power Delivery*, *33*(6), 3065–3074.

He, J., & Zhang, B. (2015). Progress in lightning impulse characteristics of grounding electrodes with soil ionization. *IEEE Transactions on Power Delivery*, *51*(6), 4924–4933.

IEEE Std. 80-2000. (2000). IEEE Guide for Safety in AC Substation Grouding.

Karami, H., & Sheshyekani, K. (2018). Harmonic impedance of grounding electrodes buried in a horizontally stratified multilayer ground: A full-wave approach. *IEEE Transactions on Electromagnetic Compatibility*, *60*(4), 899–906.

Karami, H., Sheshyekani, K., & Rachidi, F. (2017). Mixed-potential integral equation for full-wave modeling of grounding systems buried in a lossy multilayer stratified ground. *IEEE Transactions on Electromagnetic Compatibility*, *59*(5), 1505–1513.

Kherif, O., Chiheb, S., Teguar, M., Mekhaldi, A., & Harid, N. (2018). Time-domain modeling of grounding systems' impulse response incorporating nonlinear and frequency-dependent aspects. *IEEE Transactions on Electromagnetic Compatibility*, *60*(4), 907–916.

Kherif, O., Chiheb, S., Teguar, M., Mekhaldi, A., & Harid, N. (2019). Investigation of horizontal ground electrode's effective length under impulse current. *IEEE Transactions on Electromagnetic Compatibility*, *61*(5), 1515–1523.

Liew, A., & Darveniza, M. (1974). Dynamic model of impulse characteristics of conentrade earths. In *Proceedings of the institution of electrical engineers*, vol. *121*(2) (pp. 123–135).

Lima, A. C. S., Magalhães, A. P. C., Rocha, P. E. D., Meyberg, R. A., & Barros, M. T. C. (2018). A noniterative approximation of a full-wave model of thin wire above and buried in a lossy ground. *IEEE Transactions on Electromagnetic Compatibility*, *60*(6), 1873–1881.

Lima, A. C. S., Moura, R. A. R., Vieira, P. H. N., Schroeder, M. A. O., & Barros, M. T. C. A. (2019). Computational improvement in grounding systems transient analysis. *IEEE Transactions on Electromagnetic Compatibility*,. https://doi.org/10.1109/TEMC.2019.2918621.

Liu, S., Sima, W., Yuan, T., Luo, D., Bai, Y., & Yang, M. (2017). Study on X-ray imaging of soil discharge and calculation method of the ionization parameters. *IEEE Transactions on Power Delivery*, *32*(4), 2013–2021.

Longmire, C. L., & Smith, K. S. (1975). *A universal impedance for soils*. Defense Nuclear Agency, pp. 1– 24.

Magalhães, A. P. C., Silva, J. C. L. V., Lima, A. C. S., & Barros, M. T. C. (2015). Validation limits of quasi-TEM approximation for buried bare and insulated cables. *IEEE Transactions on Electromagnetic Compatibility*, *57*(6), 1690–1697.

Mazzetti, C., & Veca, G. M. (1983). Impulse behavior of grounded electrodes. *IEEE Transactions on Power Apparatus and Systems*, *102*(9), 3148–3156.

Mokhtari, M., & Gharehpetian, G. B. (2018). Integration of energy balance of soil ionization in CIGRE grounding electrode resistance model. *IEEE Transactions on Electromagnetic Compatibility*, *60*(2), 402–413.

Otani, K., Baba, Y., Nagaoka, N., Ametani, A., & Itamoto, N. (2014). FDTD surge analysis of grounding electrodes considering soil ionization. *Electric Power Systems Research*, *113*, 171–179.

Otero, A. F., Cidras, J., & Alamo, J. L. (1999). Frequency-dependent grounding system calculation by means of a conventional nodal analysis technique. *IEEE Transactions on Power Delivery*, *14*(3), 873–878.

Portela, C. M. (1999). Measuring and modeling of soil electromagnetic behavior. In *Proceedings of the IEEE 1999 international symposium on electromagnetic compatibility*. EMC Society, Seatle, USA.

Ramamoorty, M., Narayana, M. M. B., Parameswaran, S., & Mukhedkar, D. (1989). Transient performance of grounding grids. *IEEE Transactions on Power Delivery*, *4*(4), 2053–2059.

Razi-Kazemi, A. A., & Hajian, M. (2018). Probabilistic assessment of ground potential rise using finite integration technique. *IEEE Transactions on Power Delivery*, *33*(5), 2452–2461.

Rizk, M. E. M., Lehtonen, M., Baba, Y., & Abulanwar, S. (2019). Performance of large-scale grounding systems in thermal power plants against lightning strikes to nearby transmission towers. *IEEE Transactions on Electromagnetic Compatibility*, *61*(2), 400–408.

Salari, J. C., & Portela, C. A. (2007). Methodology for electromagnetic transients calculation–An application for the calculation of lightning propagation in transmission lines. *IEEE Transactions on Power Delivery*, *22*(1), 527–536.

Schroeder, M. A. O., Barros, M. T. C., Lima, A. C. S., Afonso, M. M., & Moura, R. A. R. (2017). Evaluation of the impact of different frequency dependent Soil models on lightning overvoltages. *Electric Power Systems Research*, *159*, 40–49.

Scott, J. H. (1966). Electrical and magnetic properties of rock and soil, Washington, USA.

Scott, J. H., Carrol, R. D., & Cunningham, D. R. (1967). Dieletric constant and electrical conductivity measurements of moist rock: A new laboratory method. *Journal of Geophisics Reserach*, *72*(20), 5101–5115.

Sekioka, S. (2019). Frequency and current-dependent grounding resistance model for lightning surge analysis. *IEEE Transactions on Electromagnetic Compatibility*, *61*(2), 419–425.

Silveira, F., & Visacro, S. (2014). Lightning-induced voltages over lossy ground: The effect of frequency dependence of electrical parameters of soil. *IEEE Transactions on Electromagnetic Compatibility*, *56*(5), 1129–1136.

Smith-Rose, R. L. (1933). The electrical properties of soils for alternating currents at radiofrequencies. *Proceedings of the Royal Society of London Series A*, *140*(841A), 359–377.

Sunjerga, A., Gazzana, D. S., Poljak, D., Karami, H., Sheshyekani, K., Rubinstein, M., et al. (2019). Tower and path-dependent voltage effects on the measurement of grounding impedance for lightning studies. *IEEE Transactions on Electromagnetic Compatibility*, *61*(2), 409–419.

Tanabe, K. (2001). Novel method for analyzing dynamic behavior of grounding systems based on the finite-difference time-domain method. *IEEE Power Engineering Review*, *21*(9), 55–57.

Tanaka, H., Baba, Y., Barbosa, C. F., Tsuboi, T., & Okabe, S. (2018). Protective effect of shield wires against direct lightning flashes to buried cables. *IEEE Transactions on Power Delivery*, *33*(4), 1628–1635.

Tsumura, M., Baba, Y., Nagaoka, N., & Ametani, A. (2006). FDTD simulation of a horizontal grounding electrode and modeling of its equivalent circuit. *IEEE Transactions on Electromagnetic Compatibility*, *48*(4), 817–825.

Velzaquez, R., & Mukhedkar, D. (1984). Analytical modeling of grounding electrodes. *IEEE Transactions on Power Apparatus and Systems*, *103*(6), 1314–1322.

Verma, R., & Mukhedkar, D. (1980). Impulse impedance of buried ground wire. *IEEE Transactions on Power Apparatus and Systems*, *99*(5), 2003–2007.

Visacro, S., & Alipio, R. S. (2012). Frequency dependence of soil parameters: Experimental result, predicting formula on the lightning response of grounding electrodes. *IEEE Transactions on Power Delivey*, *27*(2), 927–935.

Visacro, S., Alipio, R. S., Pereira, C., Guimarães, M., & Schroeder, M. A. O. (2014). Lightning response of grounding grids: Simulated and experimental results. *IEEE Transactions on Electromagnetic Compatibility*, *56*(5), 1163–1171.

Visacro, S., Alipio, R. S., Vale, M. H. M., & Pereira, C. (2011). The response of grounding electrodes to lighting currents: The effect of frequency dependent soil resistivity and permittivity. *IEEE Transactions on Electromagnetic Compatibility*, *53*(2), 401–406.

Visacro, S., & Portela, C. (1992). Modelling of earthing systems for lightning protection applications, including propagation effects. In *Proceedings of conference on lightning protection (ICLP)* (pp. 129-132).

Visacro, S., & Silveira, F. (2015). The impact of the frequency dependence of soil parameters on the lightning performance of transmission lines. *IEEE Transactions on Electromagnetic Compatibility*, *57*(3), 434–441.

Visacro, S., & Silveira, F. (2016). Lightning performance of transmission lines: Requirements of tower-footing electrodes consisting of long counterpoise wires. *IEEE Transactions Power Delivery*, *31*(4), 1524–1532.

Visacro, S., & Silveira, F. H. (2004). Evaluation of current distribution along the lightning discharge channel by a hybrid electromagnetic model. *Journal of Electrostatics*, *60*(2–4), 111–120.

Visacro, S., & Soares, A. (2005). HEM: A model for simulation of lightning-related engineering problems. *IEEE Transactions on Power Delivery*, *20*(2), 1206–1208.

Visacro, S., Soares, A., & Schroeder, M. A. O. (2002). An interactive computational code for simulation of transient behavior of electrical system components for lightning currents. In *26th international conference on lightning protection (ICLP). 9b.3*, Cracow, Poland, September 2–6.

Publisher's Note Springer Nature remains neutral with regard to jurisdictional claims in published maps and institutional affiliations.